Applying the Adjoint Method for Biogeochemical Modeling: Export of Particulate Organic Matter in the World Ocean

Reiner Schlitzer

Alfred Wegener Institute for Polar and Marine Research, Bremerhaven, Germany

The oceanic distributions of oxygen, dissolved nutrients and carbon are strongly affected by the production of particulate material near the ocean surface and its subsequent remineralization during sinking or after deposition on the sea-floor. Dissolved nutrient data can thus be used to derive the rate constants of biogeochemical processes responsible for the observed fields using inverse modeling. Here, a global ocean circulation model is presented that exploits the existing large sets of hydrographic, oxygen, nutrient and carbon data and determines rates of export production and vertical particle fluxes that are compatible with the concentration data. The model is fitted to the property concentration data by systematically varying circulation, air-sea fluxes, production and remineralization rates simultaneously. The adjoint method is applied as an efficient tool for the iterative optimization procedure and produces simulated property fields that are in very good agreement with measurements. The globally integrated export flux of particulate organic matter necessary for the realistic reproduction of nutrient observations is significantly larger than export estimates derived from primary productivity maps. Discrepancies are largest in oligotrophic, open-ocean areas, where the model export fluxes are up to a factor 6 higher than values based on primary productivity estimates of *Berger* [1989]. This model result is in line with a recent investigation in the subtropical North Pacific that also revealed high open-ocean fluxes. Model export production values are in much closer agreement with estimates based on satellite pigment data in most regions except in the Southern Ocean, where the satellite derived export fluxes seem to underestimate the carbon export significantly.

1. INTRODUCTION

Biogeochemical processes in the ocean strongly affect marine nutrient, carbon and oxygen distributions and act as a pump [*Volk and Hoffert,* 1985] producing vertical concentration gradients with low nutrient and carbon levels in surface water and high concentrations below. The low surface concentrations are caused by biological productivity in the sun-lit euphotic zone which uses the dissolved nutrients for the formation of particulate material (primary production PP). A fraction of the particles sinks out of the euphotic zone (export production EP), and nutrients are subsequently returned to the dissolved pool in intermediate, deep and bottom waters by particle decomposition (remineralization) during sinking in the water column or after settling on the sea-

Inverse Methods in Global Biogeochemical Cycles
Geophysical Monograph 114

floor. The lowering of surface water carbon concentrations due to the biological pump is a crucial factor that determines surface water pCO_2 values and ultimately controls atmospheric CO_2 concentrations.

Because of the large potential impact on the atmospheric CO_2 budget and on global climate, determining the strength of the biological pump, e.g., the magnitude of the export flux, has been a high priority research goal for a long time. Two main experimental approaches have been developed: (1) the direct measurement of the vertical particle flux with moored or drifting sediment traps [*Honjo et al.,* 1982; *Deuser et al.,* 1995; *Wefer et al.,* 1982] and (2) estimation of primary or export production from surface water chlorophyll concentrations obtained from satellites [*Antoine et al.,* 1996].

Sediment trap measurements are point measurements and are strongly influenced by the large temporal and spatial variability of production and particle flux events [*Wefer et al.,* 1982; *Deuser et al.,* 1995; *Fischer et al.,* 1988]. Therefore, mean export production rates for larger regions or on global scale, as required for climate studies, are difficult to obtain from trap data. Also, results from shallow traps (needed to estimate the export flux) have been questioned because of suspected low trapping efficiency. Satellite observations provide a global view, however, estimates of export fluxes from satellites have large uncertainties because the optical sensors only probe a thin surface layer and deeper chlorophyll maxima often found by towed instruments are missed. Additionally, the conversion of chlorophyll concentrations into vertical particle fluxes is difficult and relies on a very limited number of regional calibration studies.

Here, a very different approach is taken to estimate marine export production and particle fluxes as functions of depth. The basic principle was proposed and applied by *Riley* [1951], who realized that the observed nutrient and oxygen distributions can be used to determine the biogeochemical rate constants that create the property distributions. In contrast to nutrient simulations using forward models (see section 3.2 below), the estimation of physical or biogeochemical rate constants from concentration data is commonly referred to as inverse calculations. Since his work, the amount and quality of available data has increased tremendously, and advances in computer technology and numerical methods now allow detailed studies on a global scale dealing with many particle species and the large variety of measured properties simultaneously.

The model strategy described below employs the adjoint method to determine flows (physics) and production as well as remineralization parameters (biogeochemistry) that explain the global hydrography and the measured concentration fields of dissolved nutrients, carbon and oxygen best. The problem is formulated as a constrained optimization and the solution is found iteratively. It should be noted that in contrast to ecosystem models [e.g., *Fasham et al.,* 1990] that attempt to describe the complicated interactions and feedbacks of biological food-webs, in the present case the processes leading to the formation and export of particles or the processes leading to their subsequent remineralization are not modeled explicitly. Instead, production or remineralization rates are only constrained by the requirement to reproduce the observed property distributions realistically.

In this paper the adjoint method is described from an application point of view. For more background information on the adjoint technique see the article by *Giering* [1999] and the literature cited in section 3.4.

2. DATA

Measurements of dissolved oxygen and nutrients in seawater are nowadays performed routinely on most oceanographic expeditions. Measurement procedures have been automated over the time, and reliability and accuracy of the data has been steadily improved. It is remarkable that even some early field programs from the 1920s have produced oxygen and phosphate values of good quality using the simple techniques and limited resources of their time. Figure 1 shows a map of stations containing quality controlled top-to-bottom phosphate observations for the global ocean. This dataset (more than 14,000 stations) is a subset of the available historical database and covers the time from 1910 to the present with the largest number of stations between 1950 and 1990. In general, data coverage is good except for inaccessible polar regions where the available data are seasonally biased with summer data dominating over few winter observations. Data density (and quality, in the case of nitrate) are poorer for silicate, nitrate, carbon and alkalinity, but still sufficient to reconstruct the respective large-scale distributions.

For an overview over nutrient fields in the ocean, Figure 2 shows temperature, salinity, oxygen, phosphate, silicate and ΣCO_2 data along the GEOSECS West Atlantic track. The plots were produced by interpolating the original GEOSECS data [*Bainbridge,* 1980] using the Ocean Data View software [*Schlitzer,* 1999]. It can be seen that, in general, concentrations of dissolved phosphate, silicate, and carbon (Figures 2d-f) are low

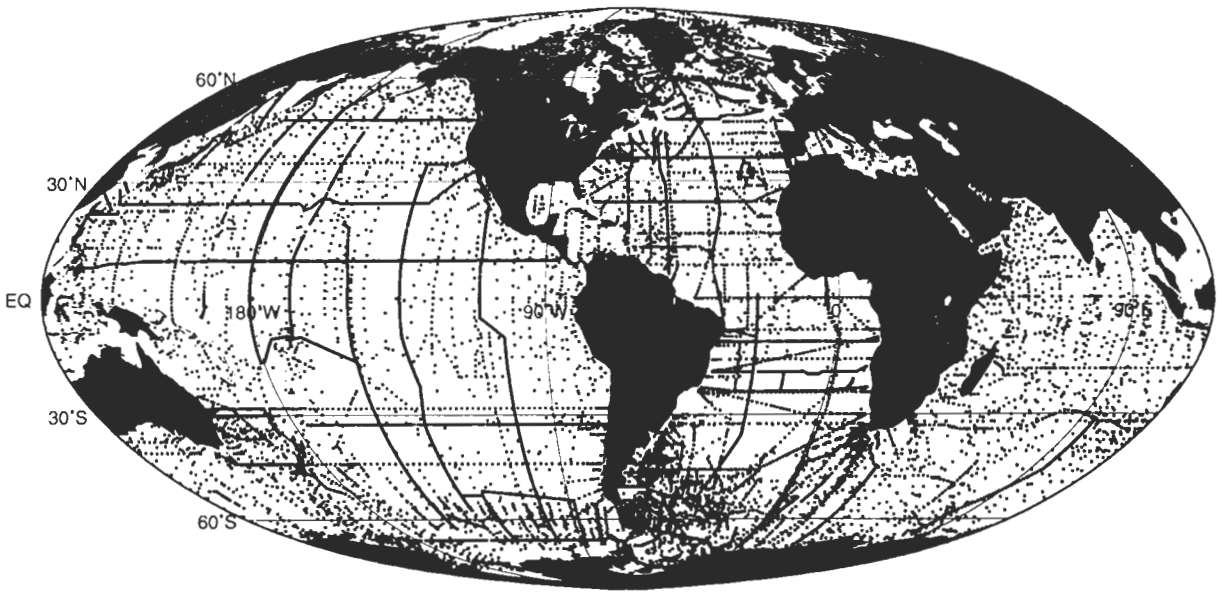

Figure 1. Map of stations with quality-controlled, top-to-bottom phosphate data.

near the surface and much higher in intermediate, deep and bottom waters. These strong vertical concentration gradients are the result of the biological pump [*Volk and Hoffert,* 1985]: biological productivity in the sun-lit euphotic zone uses dissolved nutrients for the formation of particulate material which sinks through the water column and is slowly remineralized at depth, thereby returning the nutrients back to the dissolved pool. The anti-correlation found between oxygen and phosphate (see the pronounced oxygen minimum between 200 and 1000 m depth in the tropics corresponding with phosphate maxima at the same locations) supports this interpretation because remineralization of organic particles not only releases phosphate but also uses oxygen.

Comparing the individual plots in Figure 2 shows that the vertical structure is different for the different nutrients. Whereas highest phosphate values (associated with low oxygen concentrations) are found in the upper part of the water column (maxima at about 700 m depth), the highest silicate and ΣCO_2 values are found near the bottom. This indicates that the depths of remineralization of organic material, opal and $CaCO_3$ differ greatly. Dissolution of organic material that affects phosphate, oxygen and ΣCO_2 but not silicate is obviously occurring mainly above 1000 m depth, but opal (affecting silicate) and $CaCO_3$ (affecting ΣCO_2 and alkalinity) seem to reach greater depths and are probably mainly remineralized after settling on the sea-floor.

Figure 2 also indicates that, in addition to the biogeochemical processes described above, the nutrient distributions are influenced by the effect of ocean circulation. This is most clearly seen for the Antarctic Intermediate Water (AAIW) which is characterized by low salinity values and relatively high nutrient concentrations in its source area. AAIW carries this signature along its northward path into the Atlantic at about 900 m depth (see low salinity tongue at this depth) and the nutrient maxima at this depth therefore must partly be due to the horizontal advection of nutrient rich water (see also section 4 below). The effect of advection is also seen for the Antarctic Bottom Water (AABW) carrying high nutrient concentrations northward and for the thick layer of North Atlantic Deep Water (NADW) between roughly 1500 and 4000 m depth transporting low nutrient characteristics southward.

In summary it can be concluded that almost a century of ocean observations has produced a large set of oxygen, nutrient and carbon data (in addition to the detailed hydrographic fields) that clearly contain the effects of biological production near the surface and particle remineralization at depth. Finding the biogeochemical fluxes and rate constants that generated the observed property distributions is a major task requiring a numerical model of the marine biogeochemical cycles that also (for reasons explained above) includes the three-dimensional ocean circulation. Such an approach is described below.

It should be noted that the method of inferring ma-

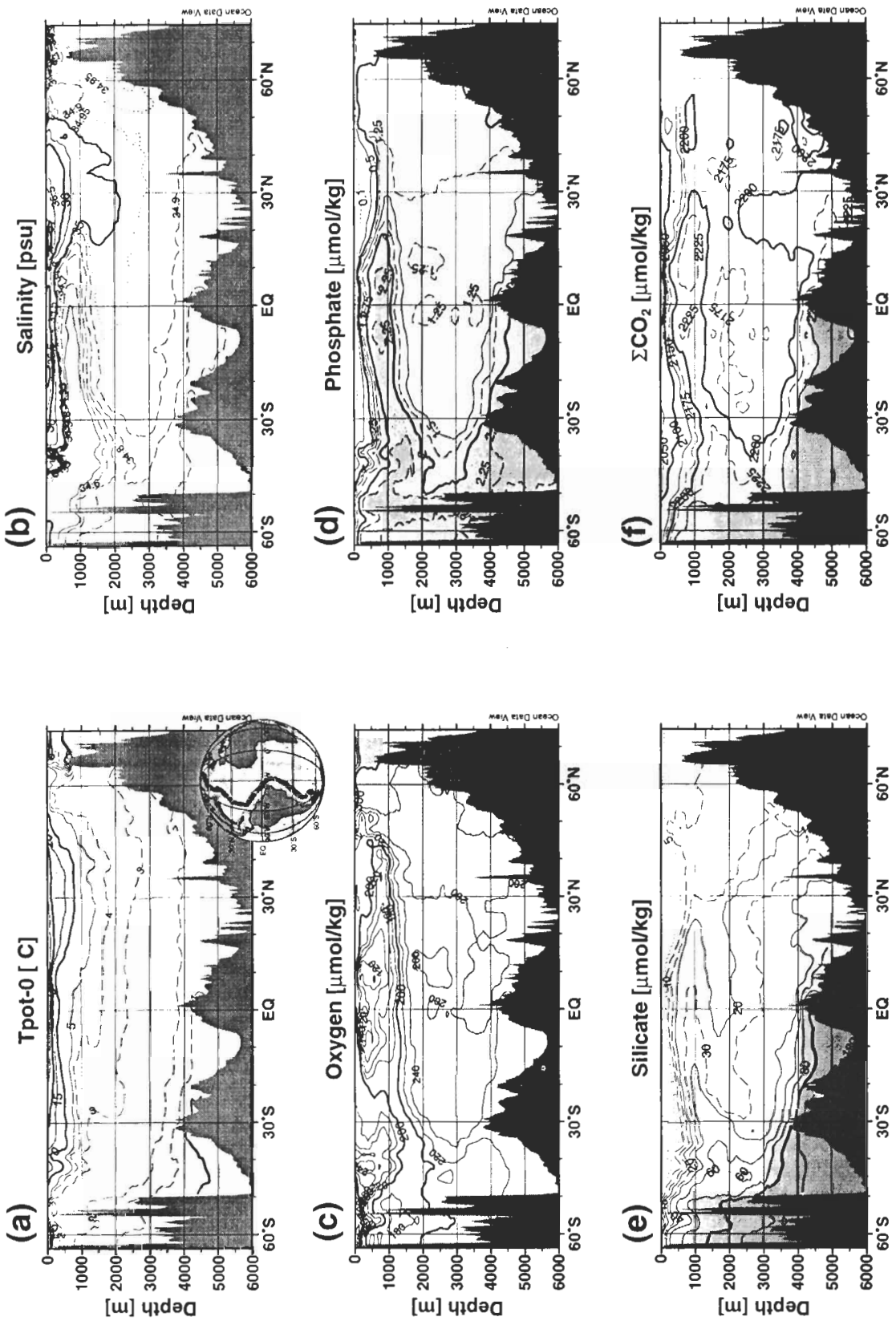

Figure 2. Hydrography and dissolved nutrient distributions along the GEOSECS West Atlantic track (redrawn using original data).

rine production rates and particle fluxes from ocean concentration data differs fundamentally from other approaches that either use direct particle flux measurements with sediment traps or ship and/or satellite observations for estimating surface productivity. Figure 3 shows oxygen profiles from two nearby stations in the tropical east Atlantic that show a pronounced oxygen minimum zone at about 500 m depth caused by remineralization of particulate organic material from the high-productivity coastal upwelling area to the east. Although there is a time-span of more than 60 years between the measurements, the observed oxygen values for the two occupations agree remarkably well, indicating that the signals in the property fields are stable over time and represent the integral response of many blooms and particle flux events over many years. This contrasts with the high spatial and temporal variability of individual production events as seen in sediment trap, ship and satellite data. Particle fluxes and productivity rates based on nutrient distributions thus represent long-term average values complementing the direct measurements from which average values can not be easily determined because of the spatial and temporal variability.

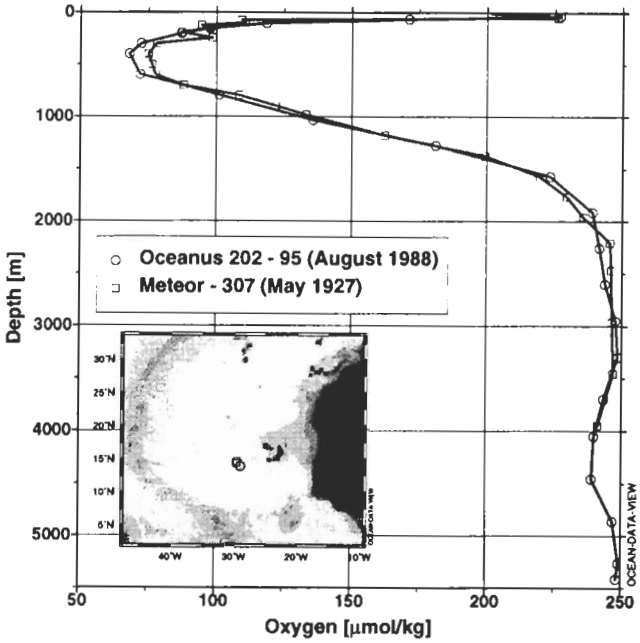

Figure 3. Oxygen profiles for two stations in the Cape Verde Basin. Note that oxygen concentrations are almost unchanged between the two occupations.

3. MODEL

As described above, determining particle fluxes and near-surface production rates from nutrient concentration data requires a biogeochemical model that also includes the ocean's 3-D circulation. Here, the global model of *Heras and Schlitzer* [1999] is used that has already been fitted to global hydrographic fields. The general model strategy is based on *Schlitzer* [1993], and more details can be found there and in *Schlitzer* [1995]. In the following, the model grid is briefly described and then the extensions with respect to biogeochemical cycling and the application of the adjoint technique for the optimization of the model are explained in detail.

Overall goal of the model calculations is to find a steady global ocean flow field (representing the climatological mean circulation) and mean export production as well as remineralization fields for three particle classes: (1) organic material (C_{org}), (2) opal and (3) $CaCO_3$. To be considered optimal, the calculated velocities must have velocity shears that are close to geostrophic shear estimates and simulations of hydrographic and nutrient distributions using model flows and biogeochemical parameters must reproduce the respective observations closely. The adjoint method provides the means that drive the model to the desired state.

3.1. Model Grid

Figure 4 shows the model grid used for the present study. Note that the grid is non-uniform with horizontal resolution ranging from 5×4 degrees longitude by latitude in open ocean areas to 2.5×2 degrees in regions with narrow currents (Drake Passage, Atlantic part of the Antarctic Circumpolar Current, Indonesian and Caribbean archipelagos), along coastal boundaries with strong currents (Florida Current, Gulf Stream, Brazil Current, Agulhas Current, Kuroshio), over steep topography (Greenland-Iceland-Scotland overflow region) and in areas with pronounced coastal up- or downwelling. In all cases the refinements are implemented in the direction of the strongest property gradients (usually perpendicular to fronts and currents) to better trace changes in ocean properties.

The model has 26 vertical layers, with thickness progressively increasing from 60 m at the surface to approximately 500 meters at 5000 m depth. Realistic topography is used, based on the U.S. Navy bathymetric data and averaged over grid-cells. Model depths over ridges and in narrow channels are adjusted manually to respective sill or channel depths. The model has three open boundaries, along which ocean properties and transports are prescribed in each model layer. They are located at the exit of the Mediterranean Sea, Red

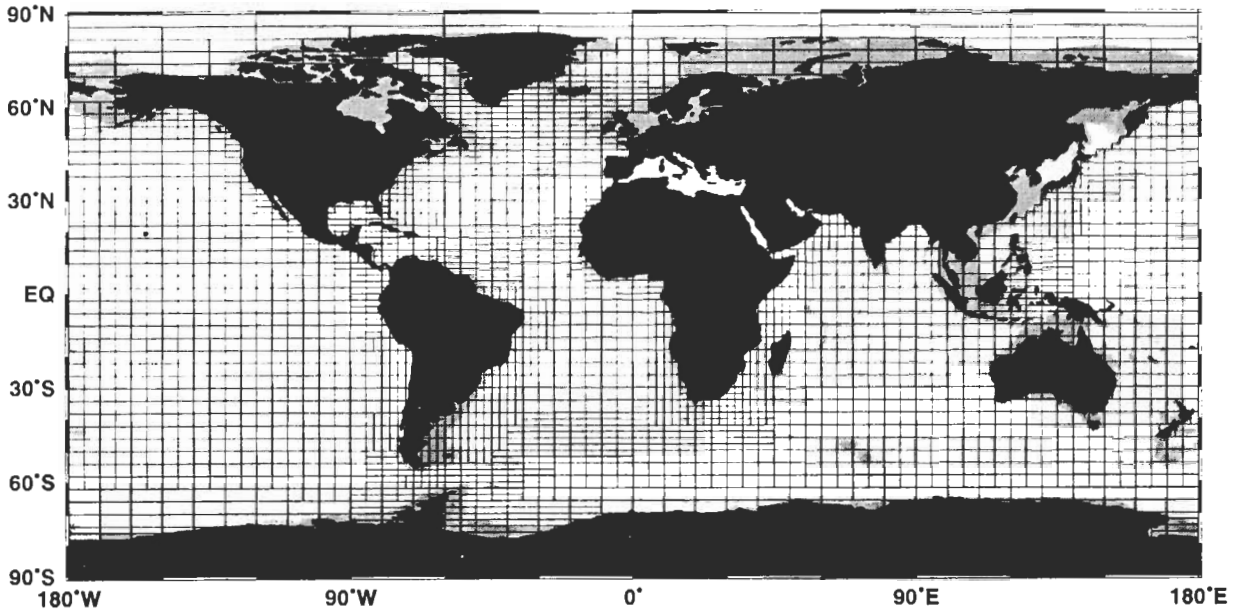

Figure 4. Variable resolution model grid used for this study. Note that resolution is increased in regions with narrow boundary currents, in coastal upwelling areas and over steep topography (bottom topography is indicated by gray-shading).

Sea and Persian Gulf. These three marginal seas are not modeled explicitly, but their impact on the global circulation is taken into account.

The model grid described above represents a compromise between the desire to resolve ocean currents and productivity patterns as closely as possible and the large computational burden imposed by the optimization procedure used to drive the model towards the observations (see below). Given present computer resources this required a relatively coarse model grid. Using variable resolution in the horizontal has the advantage to allow better representation of smaller scale features at least in some crucial parts of the model domain without the need to accommodate the higher resolution over the whole model domain. Overall, resolution of the present model is much coarser compared to eddy-resolving dynamical models but is comparable to or better than that used in other models applied for global ocean biogeochemical and circulation studies [*Yamanaka and Tajika,* 1996; *Maier-Reimer,* 1993; *Rahmstorf,* 1995].

3.2. Model Parameters and Equations

A schematic diagram of a vertical model column extending from the sea-surface down to the respective bottom depth is shown in Figure 5. Model property values are defined at the centers of the grid-boxes whereas flows are defined on the interfaces (Arakawa C-grid). Formation of particulate material is occurring in the top two model layers with the top layer contributing 75% and the second layer contributing 25% of the total production. The bottom of the second model layer is considered the base of the euphotic zone (here: z_{EZ}=133 m). Particle fluxes below the euphotic zone are assumed to decrease with depth according to

$$j_P(z) = a(z/z_{EZ})^{-b} \tag{1}$$

This functional relationship is commonly used for organic material [*Suess,* 1980; *Martin et al.,* 1987; *Bishop,* 1989], here it is also applied for opal and $CaCO_3$. In (1) a is the particle flux at the base of the euphotic zone, z_{EZ}, and represents the export production. The parameter b determines the shape of particle flux profile and thus controls the depth of remineralization. Large values for b correspond to steep particle flux decreases and thus large remineralization rates just below the euphotic zone, whereas values for b close to zero result in almost constant particle fluxes with depth with little remineralization in the water column and most of the particle export reaching the ocean floor.

In the model, export production a and remineralization scale height b may vary from grid column to grid column and independent parameter sets are used for each of the particle classes C_{org}, opal and $CaCO_3$. Note that the productivity and remineralization parameters

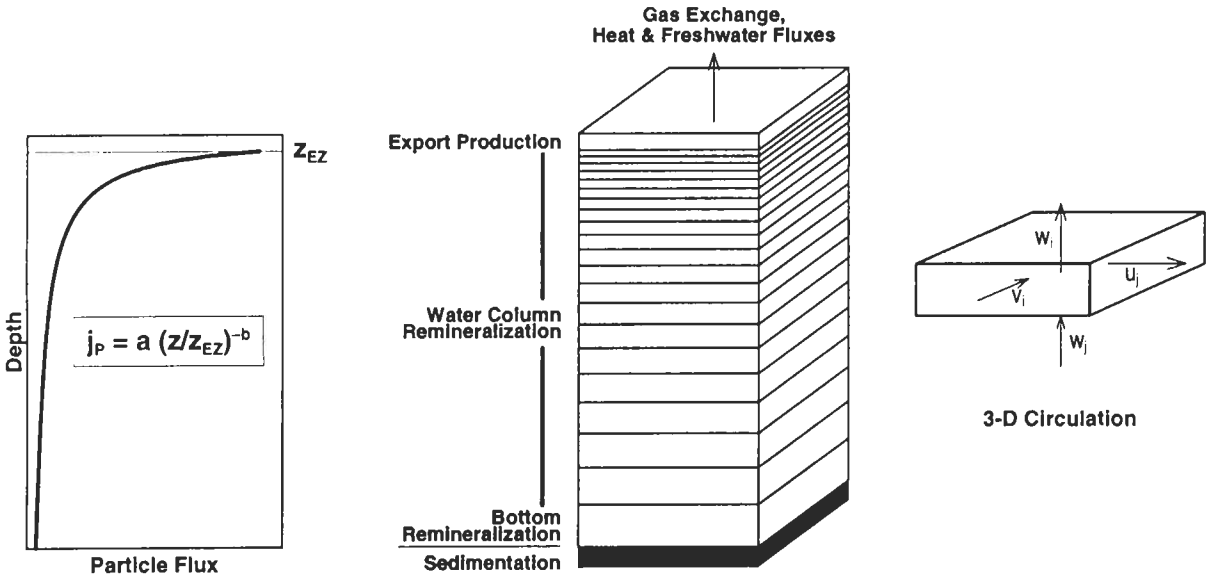

Figure 5. Vertical model grid and definition of model parameters.

a and b are not parameterized using, for instance, nutrient availability, light intensity or density stratification as in other studies [*Yamanaka and Tajika,* 1996; *Maier-Reimer,* 1993], but can be freely chosen by the model to achieve optimality (to be defined below).

The entire set of control variables (independent parameters) ultimately to be determined by the model

$$\mathbf{x} = [u, v, p_{kh}, p_{kv}, \alpha, \beta, Q_H, Q_O, Q_C]^T \qquad (2)$$

consists of horizontal flows u and v, isopycnal and diapycnal mixing parameters p_{kh} and p_{kv}, export production parameters α, remineralization parameters β, air-sea heat fluxes Q_H, air-sea oxygen gas-exchange rates Q_O and air-sea CO_2 gas-exchange rates Q_C. Quantities a and b in (1) are related to model parameters α and β in (2) by $a = \alpha^2$ and $b = \beta^2$ to assure positive values for a and b (mixing coefficients $K_h = p_{kh}^2$ and $K_v = p_{kv}^2$ are expressed by model mixing parameters p_{kh} and p_{kv} for the same reason). For the present model the total number of independent (adjustable) parameters amounts to 102,306, about 80% of them velocity parameters u and v and 20% biogeochemical and air-sea flux parameters.

Steady-state conservation equations for mass, heat, salt, phosphate, oxygen, nitrate, silicate, ΣCO_2, and alkalinity (TALK) for every model box (property budgets) comprise the set of model equations $E_i = 0$ satisfied exactly by the model (hard constraints). These equations link the set of independent model parameters $\mathbf{x}$ with a set of dependent parameters (predictions)

$$\mathbf{y} = [w, \theta, s, \mathrm{PO_4}, \mathrm{O_2}, \mathrm{NO_3}, \mathrm{SiO_2}, \Sigma\mathrm{CO_2}, \mathrm{TALK}]^T \qquad (3)$$

consisting of vertical flows w, model simulated potential temperatures θ, salinities s, phosphate PO_4, oxygen O_2, nitrate NO_3, silicate SiO_2, carbon ΣCO_2 and alkalinity TALK.

Given a set of independent parameters $\mathbf{x}$, the dependent parameters $\mathbf{y}$ are uniquely determined by the model equations. The vertical velocities w (fresh water fluxes at the air-sea interface are represented by w at the top interface) follow from the continuity equation

$$\sum_i A_i u_i + \sum_j A_j v_j + \sum_k A_k w_k = 0 \qquad (4)$$

where u_i, v_i and w_i are horizontal and vertical velocities, A_i, A_j and A_k are interface areas with positive or negative sign depending on orientation, summation is over all zonal, meridional and vertical interfaces (number of summands may vary because of the irregular grid) and w is zero at the bottom.

The steady-state property budgets include advective and diffusive transports and have the general form

$$\sum_i A_i(u_i c_i^* - K_h \Delta c_i / L_i) +$$
$$\sum_j A_j(v_j c_j^* - K_h \Delta c_j / L_j) +$$
$$\sum_k A_k(w_k c_k^* - K_v \Delta c_k / L_k) - q = 0 \qquad (5)$$

Table 1. Summary of different types of terms contributing to the cost function J, ranked in order of importance (weight).

Meaning	Mathematical Form
Deviations from geostrophic shear	$[(\zeta - \zeta_g)/(w_p \sigma_{\zeta_g})]^4$
Deviations from data (boxwise)	$[(\zeta_m - \zeta_d)/\sigma_d]^2$
Deviations from data (neighborhood average)	$[\sum_{NH}(\zeta_m - \zeta_d)/\sigma_d]^2$
Deviations from *a priori* values	$[(\zeta - T)/\sigma_T]^2$
Smoothness in zonal and meridional directions	$[\zeta_e - 2\zeta + \zeta_w]^2 + [\zeta_n - 2\zeta + \zeta_s]^2$

where again u_i, v_i and w_i are horizontal and vertical velocities, A_i, A_j and A_k are signed interface areas depending on orientation and summation is over all interfaces of a box. c^* is the property concentration on a given interface expressed as weighted-average of box concentrations on the "upwind" (c_u) and "downwind" (c_d) sides of the interface: $c^* = f_u c_u + (1 - f_u)c_d$. For this study, a weight factor $f_u = 0.7$ was chosen, resulting in a weighted-mean discretization scheme that combines the numerical robustness of the upwind scheme ($f_u = 1$) with the low artificial mixing of the centered-in-space approach ($f_u = 0.5$). K_h and K_v are horizontal and vertical mixing coefficients proportional to the squares of the respective independent parameters p_{kh} and p_{kv}. Δc are property differences between the two adjacent boxes and L is the distance between the two box centers. Finally, the source/sink term q contains fluxes across "wet" model boundaries, air-sea heat and gas-exchange fluxes and biogeochemical sinks due to formation of particulate material in the euphotic zone and biogeochemical sources due to particle remineralization below the euphotic zone. Note that $q = q(\mathbf{x})$ is a function of the independent parameters $\mathbf{x}$.

Formulation of budget equations (5) for a given property for all N_b boxes of the model results in a set of N_b linear equations for the N_b unknown box property concentrations in $\mathbf{c}$:

$$\mathbf{Ac} = \mathbf{q} \tag{6}$$

where $\mathbf{A}$ is the square advection/diffusion transport matrix containing terms of the form $A(u - K/L)$. For boxes that are only weakly coupled to the rest of the model by advective transports (e.g., boxes in isolated deep troughs) mixing coefficients are set to a high value to assure full rank of $\mathbf{A}$. Note that the transport matrix is the same for all eight properties considered in the present study and that the respective budget equations only differ in the boundary fluxes and source/sink terms contained in the right-hand-side $\mathbf{q}$. (6) is solved for the unknown concentrations (dependent parameters) $\mathbf{c}$ using a sparse LU factorization algorithm [*Harwell,* 1995]. When solving many linear systems with the same matrix, LU factorization is an efficient method because the costly factorization step has to be performed only once while the results of the factorization can be used repeatedly for the cheap solving step. Availability of the LU factor matrices also allows efficient solving of associated linear systems involving the transpose of $\mathbf{A}$, as needed for the adjoint model (see below).

3.3. Cost Function

Once the complete set of model parameters $\mathbf{p} = [\mathbf{x}, \mathbf{y}]^\mathbf{T}$ consisting of the independent parameters $\mathbf{x}$ and the dependent parameters $\mathbf{y}$ is calculated, the current model state is evaluated by calculating the value of a scalar cost function. The cost function J accumulates penalties for all undesired features of the model solution. A large value of the cost function indicates that the current model solution is far from the desired state, and goal of subsequent model runs is to minimize the value of J, thereby forcing the model in the wanted direction.

The characteristics of the desired model solution are determined by the form of the cost function, and definition of J is an important step during model setup. Note that in contrast to the model equations $E_i = 0$ that are satisfied exactly by the model (hard constraints), the principles expressed in cost function terms act as weak or "soft" constraints and, in general, the cost function and most of its individual terms remain non-zero. The most important terms contributing to the cost function of the present study are discussed in the following and a summary of the different types of terms and their mathematical form is given in Table 1.

3.3.1. Deviations from geostrophic velocity shear estimates. Unlike dynamical models, the present approach does not solve the Navier-Stokes equation in order to calculate model velocities. Instead, the geostrophic approximation is implemented using a cost function term

that adds penalties if vertical shears of model velocities ζ differ from geostrophic shears ζ_g estimated on the basis of the original hydrographic data (w_p is a profile dependent weight that is large in areas of poor data coverage and σ_{ζ_g} is an error estimate for the geostrophic shear). The geostrophic shear deviations are raised to power 4 to avoid occasional large misfits that appeared when using a power 2 formulation. Constant offsets of the velocity profiles, corresponding to the unknown reference velocities of the geostrophic method, are not penalized and can arbitrarily be chosen by the model. A large weight on this term assures that model velocities indeed stay close to geostrophic estimates [*Heras and Schlitzer,* 1999; *Schlitzer,* 1996].

3.3.2. Deviations from data. If model simulated property fields ζ_m for temperature, salinity, phosphate, oxygen, silicate, ΣCO_2 and TALK deviate from corresponding measurements ζ_d, penalties are added to the cost function J by means of two different terms (Table 1). The first one is a boxwise comparison of model and data values, normalized by the data error σ_{ζ_d} and then squared, while the second form averages the normalized deviations over a given box and all of its neighbors and adds the squared average deviation to the cost function. The latter contribution is large if the simulated fields show systematic differences compared to the data over larger than grid-size dimensions while it is small if deviations within the neighborhood are random. This second term proved very successful for minimizing large-scale systematic property offsets.

3.3.3. Deviations from a priori values. Well known oceanographic transports T are imposed on the model by penalizing differences to respective model equivalent transports ζ: (a) Florida current 30 Sverdrup (1 Sv = 10^6 m^3 s^{-1}); (b) Drake Passage throughflow 130 Sv; (c) North Atlantic Deep Water (NADW) transport across equator -18 Sv; (d) transport through the Indonesian archipelago from the Pacific to the Indian Ocean 10 Sv; (e) export of Arctic waters to Baffin Bay 1 Sv; and (f) flow through Bering Strait into the Arctic Ocean 0.8 Sv.

3.3.4. Smoothness constraints. Horizontal smoothness of vertical velocities w, export production rates a, remineralization scale-heights b and gas-exchange rates Q_O and Q_C is enforced by terms penalizing the second derivatives of these properties in zonal and meridional directions. Note that second derivatives are approximated using five-point finite differences in east-west and north-south directions, respectively.

Choosing weight factors for all the different terms of the cost function is not straightforward and introduces a certain degree a subjectivity that influences the final solution sought by the model. In the present case largest weights were used for the geostrophic constraint and the deviations from observed fields. The weights for the smoothness constraints were chosen much smaller such that the respective terms were more than one order of magnitude smaller than the others.

3.4. Adjoint Model

In mathematical terms, the problem to be solved is an optimization problem with equality constraints

$$\begin{aligned} & min \quad J(\mathbf{p}) \qquad (\mathbf{p} \in \mathbb{R}^n) \\ \text{subject to} \quad & E_i(\mathbf{p}) = 0 \qquad (i = 1, ..., n_e) \end{aligned} \tag{7}$$

with $n = n_i + n_d$ the total number of independent and dependent parameters and n_e the total number of model equations E_i representing the property budget equations (6) of the model in the form $\mathbf{Ac} - \mathbf{q} = \mathbf{0}$ (note that $n_e = n_d$). Because the model equations E_i are non-linear in parameters $\mathbf{p}$, the solution can not be calculated directly but must be found iteratively (see [*Hestenes,* 1975; *Gill et al.,* 1981; *Bertsekas,* 1982; *Luenberger,* 1984; *Bertsekas,* 1995;] for theoretical and applied aspects of optimization problems).

The general procedure for finding the optimal solution of constrained minimization problems is as follows: given a current model state $\mathbf{p_i} \in \mathbb{R}^n$, the gradient of the cost function J with respect to the independent parameters $\mathbf{x}_i$ is calculated and passed to a descent algorithm that produces a new set of independent parameters $\mathbf{x}_{i+1}$. Then, the corresponding dependent parameters $\mathbf{y}_{i+1}$ are calculated using the model equations $E = 0$ and a new, improved model state $\mathbf{p}_{i+1}$ with a smaller value of cost function $J_{i+1} < J_i$ is found. This completes one iteration of the procedure, and usually many iterations are required until a conveniently chosen stopping criteria is met and a minimum of J is found.

Calculating the gradient of J with respect to $\mathbf{x}_i$ is a nontrivial task and it is here where the adjoint method (also called "method of Lagrange multipliers") comes into play. It turns out that using this method the gradient can be calculated at a computational cost equivalent to only one forward run, instead of the n_i forward runs that would be needed if all the n_i components were calculated by means of individual perturbation analysis runs. Thus, the adjoint is seen to be a very efficient method producing the cost function gradient needed for every iteration of the procedure. The following description of the adjoint method is based on *Thacker and Long* [1988] and *Thacker* [1988].

Starting with the cost function J of the problem, the Lagrange function L is defined as

$$L = J + \sum_{j=1}^{n_e} \lambda_j E_j \tag{8}$$

where n_e is the number of model equations $E_j = 0$, and λ_j are corresponding, yet undetermined Lagrange multipliers. Like J, L is a scalar function, but in addition to the model parameters $\mathbf{p}$ it also depends on the Lagrange multipliers λ. Optimization theory proves that a minimum point $\mathbf{p}$ of J is a stationary point of L, e.g., all partial derivatives of L with respect to Lagrange multipliers λ_i, dependent parameters $\mathbf{y}$ and independent parameters $\mathbf{x}$ vanish at $\mathbf{p}$

$$\frac{\partial L}{\partial \lambda_j} = E_j = 0 \tag{9}$$

$$\frac{\partial L}{\partial y_i} = \frac{\partial J}{\partial y_i} + \sum_{j=1}^{n_e} \lambda_j \frac{\partial E_j}{\partial y_i} = 0 \tag{10}$$

$$\frac{\partial L}{\partial x_i} = \frac{\partial J}{\partial x_i} + \sum_{j=1}^{n_e} \lambda_j \frac{\partial E_j}{\partial x_i} = 0 \tag{11}$$

Differentiation with respect to the Lagrange multipliers (9) recovers the model equations $E_j = 0$, and differentiation with respect to the dependent and independent model parameters y_i and x_i yields the *adjoint equations* (10) and (11). Seeking the minimum of J then is equivalent to finding a model solution that satisfies (9), (10) and (11). In practice, a minimum point of J is approached by an iterative procedure. Given a current model state, the Lagrange multipliers λ are calculated by solving (10) with $\partial L/\partial y_i$ set to zero. Introducing the λ into (11) then yields the gradient of L with respect to the independent parameters $\partial L/\partial x_i$. This gradient of L is then passed to a descent algorithm (here: limited memory, quasi-Newton conjugate gradient algorithm [*Gilbert and Lemaréchal,* 1989]) to obtain a new, improved set of independent model parameters $\mathbf{x}$ that will produce a smaller value of L and the cost function J.

The values of the Lagrange multipliers at the minimum point provide useful information on the sensitivity of the cost function J to perturbations in the model equations. If, for instance, a residual δ_i is allowed for the i-th model equation ($E_i = \delta_i$), then the resulting change of J is proportional to the Lagrange multiplier λ_i associated with this equation. Inspection of the sizes of the λ_i thus reveals the relative importance of the individual model equations in determining the magnitude of the cost function and they indicate by how much J would change if certain residuals in the model equations would be tolerated.

In the present case (10) represents a square system of $n_d = n_e = 9N_b = 399,492$ linear equations in the n_e unknown Lagrange multipliers λ_j. This linear system can be separated into nine smaller independent linear systems of dimension N_b because a given property (model temperatures, salinities, etc.) appears only in the N_b budget equations for this property and does not influence the budget equations of the other properties. Thus, the vector of Lagrange multipliers λ can be calculated by sequentially solving these smaller systems. Inspection of the property budget equations (5) shows that the sub-systems of (10) to be solved for each property can be written as

$$\mathbf{A}^T \lambda = -\frac{\partial J}{\partial \mathbf{y}} \tag{12}$$

where $\mathbf{A}^T$ is the transpose of the advection/diffusion transport matrix (note that the concentrations c_i in (5) represent the dependent parameters y_i in (10)). Because the LU factorization of $\mathbf{A}$ is available from the step calculating the property concentrations $\mathbf{c}$, solving (12) for the unknown Lagrange multipliers is computationally very cheap.

Overall, the model calculations proceed according to the following steps (see Figure 6):

(S0) Initialize the independent parameters $\mathbf{x}$ (here, horizontal flows u and v were set to the geostrophic flows calculated from hydrographic data, all other parameters were set to first guess values taken from the literature or chosen arbitrarily: (a) export production parameters a for organic material were initialized using maps of primary productivity [*Berger,* 1989; Figure 7] and empirical relationships linking particle export with primary production [*Eppley and Peterson,* 1979], (b) remineralization parameters b were set to 1 [*Suess,* 1980], and (c) O_2 and CO_2 gas-exchange rates were initially set to zero).

(S1) Calculate dependent parameters $\mathbf{y}$ using steady-state property budgets (5).

(S2) Calculate the value of the cost function J.

(S3) Calculate the gradient $\partial L/\partial x$ by solving the adjoint equations (10) and (11).

(S4) Use $\partial L/\partial x$ from S3 in a descent algorithm to obtain a new, improved set of independent model parameters $\mathbf{x}$.

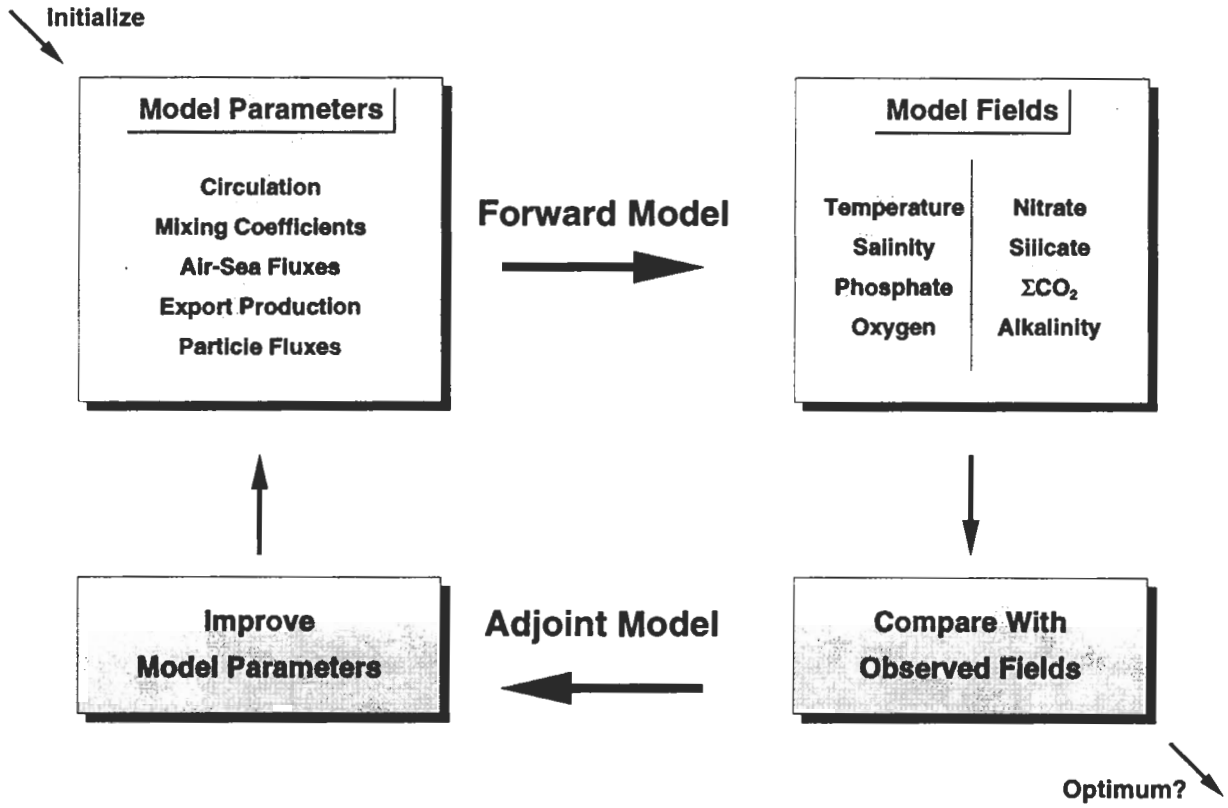

Figure 6. Schematic overview of model calculations performed for every iteration of the optimization process.

(S5) Back to S1 unless a stopping criteria, indicating that the current point is sufficiently close to a minimum of the cost function J, is met.

Step S1 is usually referred to as running the "forward model". Its most computationally intensive part is calculation of the model property fields, which involves solving large (but sparse) sets of linear equations. The calculation of the w is comparatively cheap. For each run of the forward model, one run of the adjoint model (step S3) is needed to complete an iteration. The computational cost running the adjoint model is comparable with running the forward model. However, if LU factorization is used for solving the budget equations (5), then solving the associated adjoint model imposes very little overhead because the factorization of the forward step can be used for the adjoint as well.

It should be pointed out that the main purpose of the adjoint model is to calculate the gradient of the cost function (a direction in parameter-space along which the cost function J decreases) efficiently. In principle, this gradient could also be calculated by perturbing a single independent parameter $x_i' = x_i + \delta x_i$ at a time and recalculating the value of the cost function J_i' for this perturbed parameter set thereby obtaining the i-th component of the gradient $\partial J/\partial x_i = (J_i' - J)/\delta x_i$. Repeating this procedure for all independent parameters then yields the full gradient vector. Regarding the large number of model parameters (here: n_i=102,306), however, this procedure is impractical because it would involve n_i runs of the forward model in order to calculate the gradient of J once. The great advantage of the adjoint formalism is, that it allows the calculation of the gradient much more efficiently, namely with an effort equivalent to only one additional forward run instead of n_i runs.

4. RESULTS

The adjoint technique described above was applied to the model of *Heras and Schlitzer* [1999] (see Figure 4) starting with their solution ExpB obtained by forcing the model to hydrographic data only. For the biogeochemical model experiment the following assumptions and approximations were made: (a) element ratios of particulate organic material are constant (P:N:C:O=

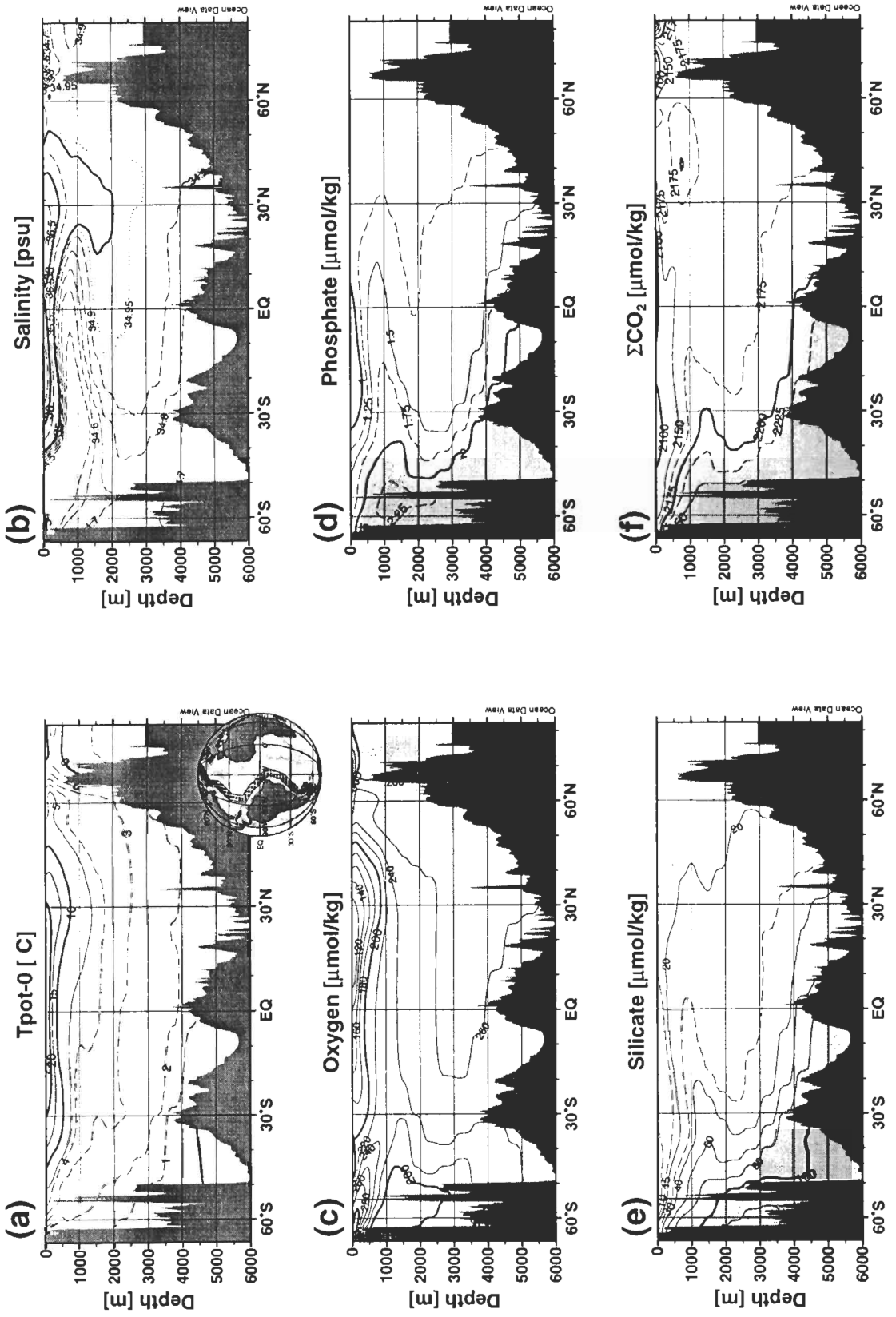

Figure 7. Model simulated hydrography and dissolved nutrient distributions along the GEOSECS West Atlantic track for an Atlantic model without particle fluxes.

1:16:106:-136; [*Redfield et al.*, 1963]), (b) nitrification/ denitrification processes are neglected, (c) no dissolved organic matter (DOM) is considered and (d) burial of particulate material as well as river-input of nutrients is neglected. The experiment has to be considered the baseline experiment, model runs with different P:N:C:O element ratios, including DOM and considering sedimentation and river input are underway.

4.1. Property Distributions

To illustrate the importance of the biological pump for the dissolved nutrient distributions in the ocean, Figure 7 shows simulated hydrography, oxygen and nutrients along the GEOSECS west Atlantic track from a version of the model covering the Atlantic only (variable resolution grid 2×1.5 to 0.5×0.5 degrees; open model boundaries across Drake Passage and between the tip of South Africa and Antarctica) and including O_2 and CO_2 gas-exchange but no particle production in the euphotic zone and remineralization below. Whereas the 3D circulation in the model is capable of reproducing the hydrography in the Atlantic closely (compare with Figure 2), deviations between simulated nutrients and oxygen and respective data (Figure 2) are large.

Without particle production phosphate, silicate and ΣCO_2 surface water concentrations are far too high, whereas sub-surface nutrient levels are generally too low. Note that in the intermediate water layer (~1000 m depth) the northward spreading AAIW produces tongues of nutrient rich water extending northward. However, for phosphate and ΣCO_2 these tongues are much weaker than in reality and the pronounced maxima north and south of the equator are missing in the simulations. Also note that the simulation fails to produce the strong sub-surface oxygen minima in tropical and sub-tropical regions found in the data. For silicate, the tongue associated with northward spreading intermediate water agrees remarkably well with observations and the largest model misfits occur in the bottom layer indicating that the missing opal remineralization mainly affects the deeper parts of the ocean.

Figure 8 shows the simulated property fields of the global model including biogeochemical cycles of particulate organic matter, $CaCO_3$ and opal. By means of the iterative optimization procedure described above the model has established fields of export production a and remineralization scale heights b as well as an appropriately adjusted flow field (shown elsewhere) that together produce oxygen and nutrient fields (in addition to hydrography) much more realistically than the model without biogeochemistry. As a consequence of biological production, surface values of nutrients are now low, and shallow oxygen minima and associated nutrient maxima due to particle remineralization are simulated with realistic spatial extent and amplitude. Also note that when opal fluxes are included, the deep silicate distribution can be brought into very good agreement with the data.

4.2. Export Production

The model export production of particulate organic matter (POM) necessary to produce the nutrient fields in Figure 8 is shown in Figure 9. The spatial pattern of model export production resembles the general pattern of primary production in published maps [*Berger*, 1989; *Antoine et al.*, 1996], showing high fluxes in coastal upwelling areas off West Africa, along the West American coast, in the Arabian Sea and Bay of Bengal, in the northwest Atlantic and north and tropical Pacific, in the area of the Indonesian archipelago and in the Southern Ocean. Highest values in the productive areas are on the order of 5 to 10 mol C m^{-2} yr^{-1}; in the oligotrophic, open-ocean regions they amount to between 0.5 and 2 mol C m^{-2} yr^{-1}.

The export of POM in the model predominantly occurs at mid-latitudes and in the Southern Ocean (474 and 331 Tmol C yr^{-1} in zonal bands 30°N - 30°S and 30°S - 90°S, respectively), and the contribution of the Northern Hemisphere is comparatively small (115 Tmol C yr^{-1} between 30°N and 90°N). Globally integrated, the POM export in the model is 920 Tmol C yr^{-1} equivalent to 11 Gt C yr^{-1}. This value is in good agreement with modeling results of *Yamanaka and Tajika*, [1996] but is more than a factor of 2 larger than a global estimate based on the primary productivity map of *Berger* [1989] (their Figure 7) and the *Eppley and Peterson* [1979] conversion formula from PP to EP.

Ratios of model export production and PP-derived export estimates are shown in Figure 10 for the primary productivity maps of *Berger* [1989] and *Antoine et al.* [1996]. Except in the Weddell Sea and the tropical East Pacific, the model export fluxes turn out to be higher than the estimates based on *Berger*'s [1989] PP values (Figure 10a). Discrepancies are largest in open-ocean areas of the Pacific, Indian Ocean and South Atlantic, where the model export is up to a factor of 6 larger than the PP-derived fluxes. In most high productivity regions (coastal regions of the East Pacific, Arabian Sea, Bay of Bengal, North Atlantic, etc.) the two estimates are more nearly comparable, and the higher global export in the model is seen to be mainly due to the more productive open-ocean areas. Compari-

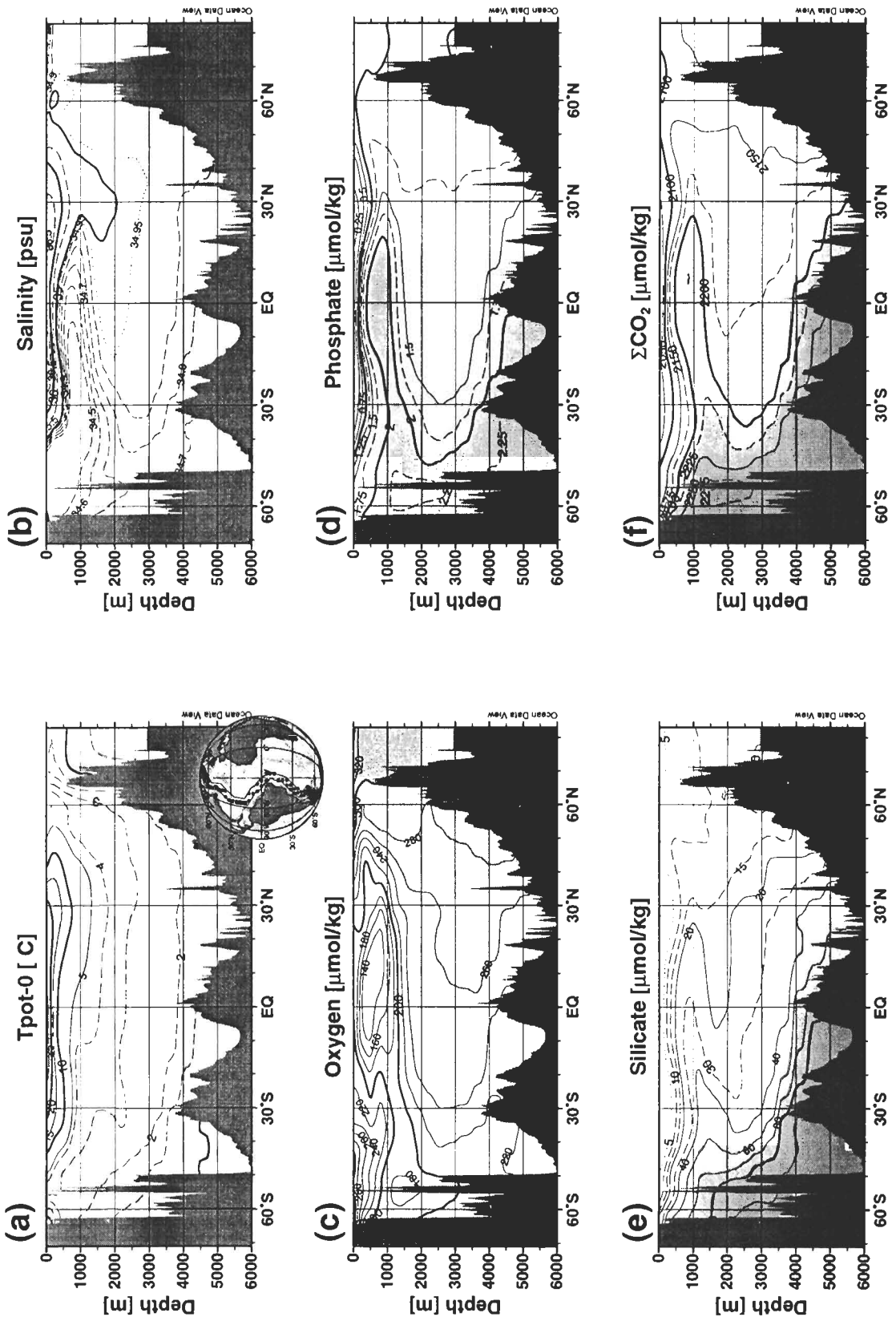

Figure 8. Optimal model simulated hydrography and dissolved nutrient distributions along the GEOSECS West Atlantic track for the global model with particle fluxes.

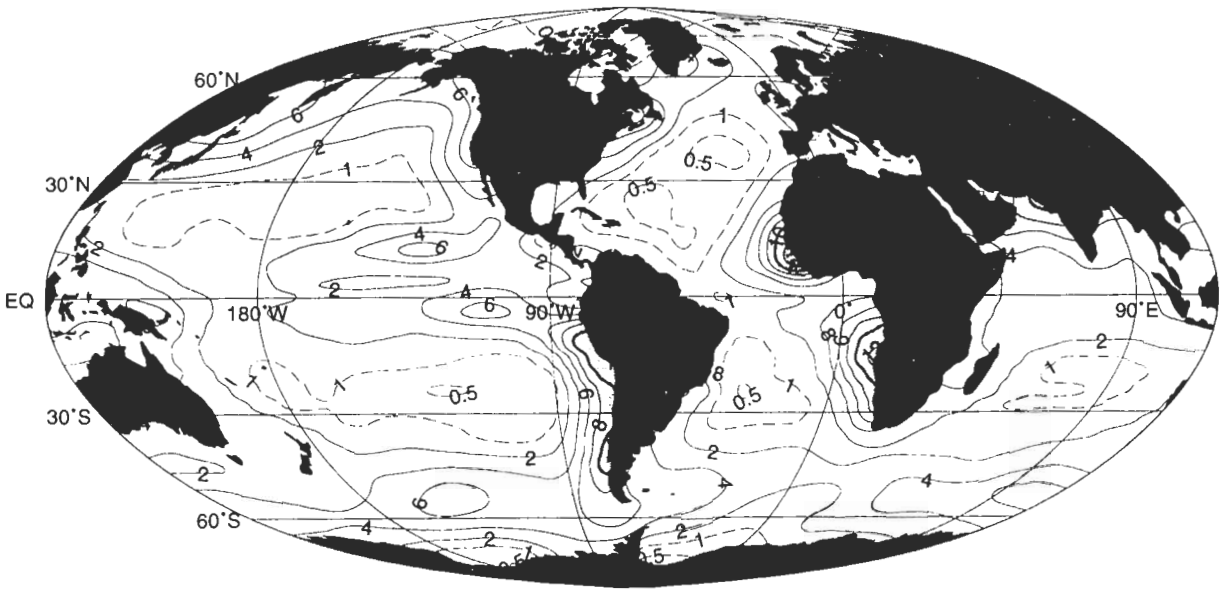

Figure 9. Export production of particulate organic matter (POM) [mol C m^{-2} yr^{-1}] for the global model.

son with export fluxes derived from satellite observations [*Antoine et al.*, 1996] (Figure 10b) also shows the model being higher, however, the differences are now much smaller and the most obvious discrepancies occur in the Southern Ocean, where the model export fluxes again are three to five times larger.

5. DISCUSSION

The model experiments presented above show that the adjoint method is a powerful tool that can be applied to a wide range of linear or non-linear constrained problems and demonstrate that even large-scale optimizations can be performed on widely available workstation computers. Whereas in the case of "forward-only" models the variation of control variables and the analysis of subsequent changes in the output variables have to done manually, and usually significant differences between data and their model counterparts remain, the adjoint method provides an automatic and systematic optimization procedure that yields simulated fields that are usually in good agreement with observations. The capability of a model to explain the data accurately is an important requirement in order to accept (and consider reliable) the final, optimal values of the control variables (here: biogeochemical rate constants).

In the present case a model solution could be found that realistically reproduces all major features in the global distributions of hydrographic parameters, oxygen, nutrients and carbon simultaneously. The export production of particulate organic material necessary to produce the observed property distributions is significantly higher than estimates based on *Berger*'s [1989] map of primary production, especially in oligotrophic, open-ocean areas. This high export production in open-ocean regions in the model is in agreement with recent, independent investigations in the subtropical northeast Pacific [*Emerson et al.*, 1997; see also *Doney*, 1997]. Based on detailed oxygen, inorganic carbon and organic carbon data, they derive a relatively high export flux of 2 ± 1 mol C m^{-2} yr^{-1} at the ALOHA time-series station (22°45'N, 150°W), a value that is in good agreement with model results in this area (Figure 9).

Compared to *Berger*'s [1989] map, the productivity estimates of *Antoine et al.* [1996] also show higher fluxes in open-ocean, oligotrophic regions and thus provide another piece of evidence for the conclusion that the vast, nutrient depleted subtropical gyres might play a greater role for the vertical carbon transport into the deep ocean and for the uptake of anthropogenic carbon by the ocean than previously thought. In the Southern Ocean south of 50°S the export fluxes derived from *Antoine et al.* [1996] are lower than model values and estimates based on the *Berger* [1989] map. This might be due to systematic biases in the satellite data that do not contain information on sub-surface chlorophyll maxima frequently observed in that area.

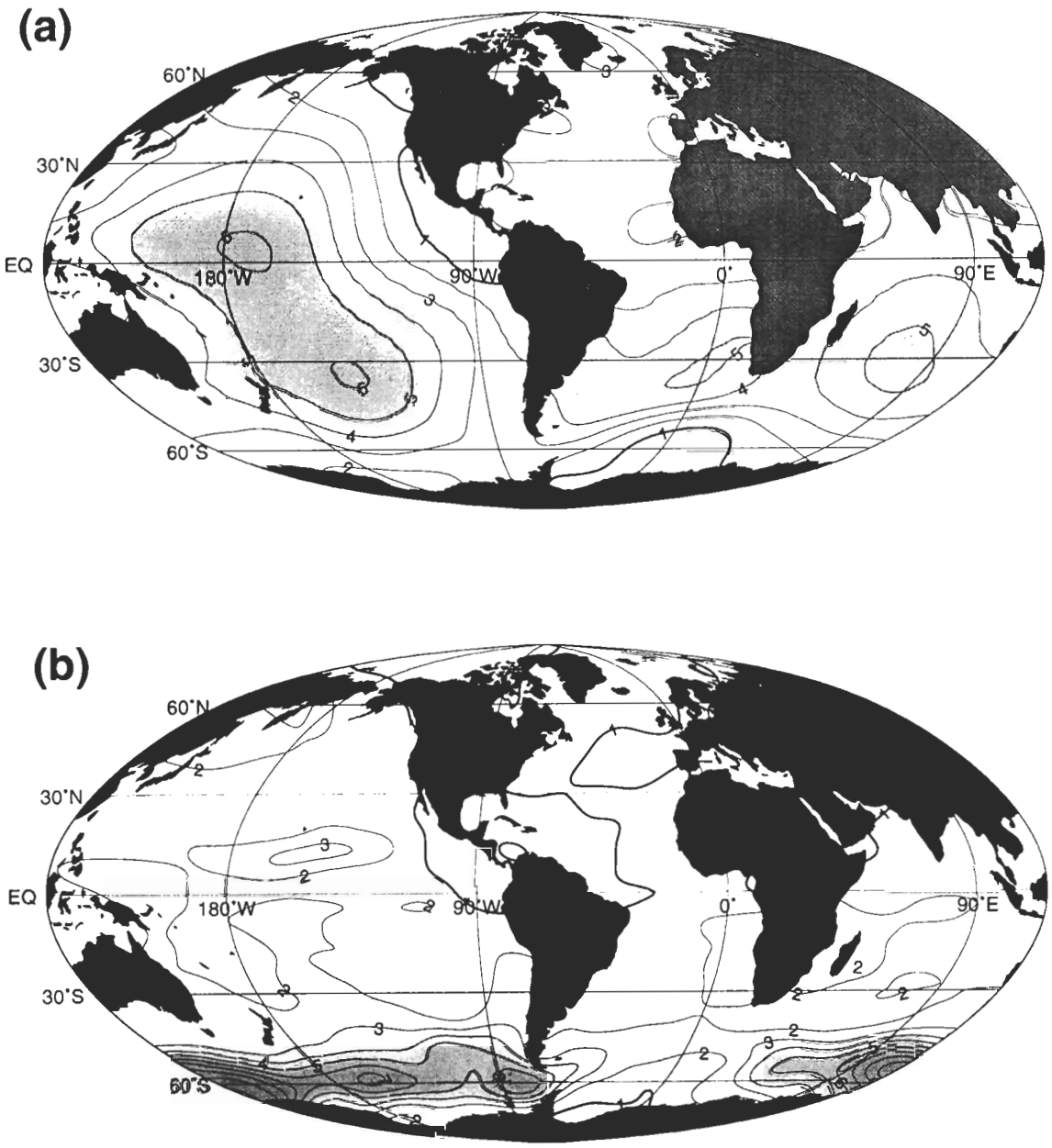

Figure 10. Ratio of model export production of particulate organic matter (POM) and values derived from primary productivity maps of (a) *Berger* [1989] and (b) *Antoine et al.* [1996]. Primary production is converted to export production using the empirical conversion formula of *Eppley and Peterson* [1979].

Concerning methodological issues for large-scale, nonlinear problems, two caveats of the adjoint method should be noted.

(1) While a minimum of the cost function J can usually be found with affordable computer resources, there is no guaranty that the minimum is a global one. New approaches like the TRUST algorithm for global optimization [*Barhen et al.*, 1997] appear to be too demanding to be applied to large-scale cases, and usually one has no choice other than trying different starting points in parameter space $\mathbf{x}$ and to determine whether identical or different solution points are approached in the different cases. In practice, only a very limited number of optimization runs can be performed and a solution is

accepted if the cost function is "sufficiently" small (although it might not represent the smallest cost function value achievable).

(2) Error analysis of the solution vector $\mathbf{x}$ of large problems is not straightforward [*Thacker*, 1989]. In principle, an eigenvector/eigenvalue analysis of the inverse Hessian matrix $\mathbf{H}$ (the Hessian is the square matrix of second partial derivatives of J with respect to parameters p_i) reveals directions in parameter space that are well determined (eigenvectors $\mathbf{u}_i$ associated with large eigenvalues; value of J increases rapidly when moving away from optimal point $\mathbf{x}$ along $\mathbf{u}_i$) and directions that are only poorly determined by the model (eigenvectors $\mathbf{u}_j$ associated with smallest eigenvalues; value of J increases slowly when moving away from optimal point $\mathbf{x}$ along $\mathbf{u}_j$). Note that the ratio of largest and smallest eigenvalues of $\mathbf{H}^{-1}$ is a measure of the anisotropy of J around $\mathbf{x}$. Whereas the required eigenvector/eigenvalue analysis can be easily performed for small optimization problems, it is impossible for large systems like the present one.

One possibility to obtain rough information on the shape of the cost function in the neighborhood of the optimal point and uncertainties for the determined parameter values is to add new, highly weighted terms to the cost function that enforce prescribed values for certain parameters (or combinations of parameters) and then investigate the change in cost function for different prescribed parameter values. This was used in *Schlitzer* [1995], *Schlitzer* [1996] and *Heras and Schlitzer* [1999] to determine the range of mixing coefficients and meridional volume as well as heat transports in the Atlantic compatible with the measured distributions of temperature and salinity. In the present case, this method could be used to find the range of, for instance, global carbon export flux or remineralization scale heights b that produce realistic nutrient distributions.

NOTATION

a	export flux
$\mathbf{A}$	advection/diffusion operator
b	particle remineralization parameter
$\mathbf{c}$	vector of property concentrations
EP	export production
E	model equations
$\mathbf{H}$	Hessian matrix
j_P	particle flux
J	cost function
K_h, K_v	horizontal and vertical mixing coefficients
p_{kh}, p_{kv}	model parameters representing horizontal and vertical mixing
POM	particulate organic matter
PP	primary production
$\mathbf{p}$	vector of independent and dependent parameters
$\mathbf{q}$	vector of source/sink terms
Q_H, Q_O, Q_C	air-sea heat, oxygen and carbon fluxes
u, v, w	zonal, meridional, and vertical velocities
$\mathbf{x}$	control variables (independent parameters)
$\mathbf{y}$	dependent parameters
z	depth
z_{EZ}	depth of euphotic zone
α	model parameter representing export flux
β	model parameter representing remineralization

Acknowledgments. This is SFB 261 contribution 277 and publication 1644 of the Alfred Wegener Institute for Polar and Marine Research.

REFERENCES

Antoine, D., J.-M. Andre, and A. Morel, Oceanic primary production 2. Estimation at global scale from satellite (coastal zone color scanner) chlorophyll, *Glob. Biogeochem. Cycl.*, *10*, 57–69, 1996.

Bainbridge, A. E., *GEOSECS Atlantic Expedition, Vol. II, Sections and Profiles 1972-1973*, U.S. Government Printing Office, Washington D. C., 1980.

Barhen, J., V. Protopopescu and D. Reister, TRUST: A deterministic algorithm for global optimization, *Science*, *276*, 1094–1097, 1997.

Berger, W. H., Global maps of ocean productivity, in *Productivity of the Ocean: Present and Past*, edited by W. H. Berger, V. S. Smetacek and G. Wefer, pp. 429–455, John Wiley, New York, 1989.

Berger, W. H., V. S. Smetacek and G. Wefer, Ocean productivity and paleoproductivity — An overview, in *Productivity of the Ocean: Present and Past*, edited by W. H. Berger, V. S. Smetacek and G. Wefer, pp. 1–34, John Wiley, New York, 1989.

Bertsekas, D. P., *Constrained Optimization and Lagrange Multiplier Methods*, 395 pp., Academic, San Diego, Calif., 1982.

Bertsekas, D. P., *Nonlinear Programming*, 646 pp., Athena Scientific, Belmont, Mass., 1995.

Bishop, J. K. B., Regional extremes in particular matter composition and flux: Effects on the chemistry of the ocean interior, in *Productivity of the Ocean: Present and Past*, edited by W. H. Berger, V. S. Smetacek and G. Wefer, pp. 117–137, John Wiley, New York, 1989.

Deuser, W. G., T. D. Jickells, P. King, and J. A. Commeau, Decadal and annual changes in biogenic opal and carbon-

ate fluxes to the deep Sargasso Sea, *Deep Sea Res.*, *42*, 1923–1932, 1995.

Doney, S. C., The ocean's productive deserts, *Nature*, *389*, 905–906, 1997.

Emerson, S., P. Quay, D. Karl, C. Winn, L.Tupas, and M. Landry, Experimental determination of the organic carbon flux from open-ocean surface waters, *Nature*, *389*, 951–954, 1997.

Eppley, R. W. and B. J. Peterson, Particulate organic matter flux and planktonic new production in the deep ocean, *Nature*, *282*, 677–680, 1979.

Fasham, M. J. R., H. W. Ducklow, and S. M. McKelvie, A nitrogen-based model of plankton dynamics in the oceanic mixed layer, *J. Mar. Res.*, *48*, 591–639, 1990.

Fischer, G., D. Fütterer, R. Gersonde, S. Honjo, D. Ostermann, and G. Wefer, Seasonal variability of particle flux in the Weddell Sea and its relation to ice cover, *Nature*, *335*, 426–428, 1988.

Giering, R., Tangent linear and adjoint biogeochemical models, this volume, 1999, American Geophysical Union.

Gilbert, J. Ch. and C. Lemaréchal, Some numerical experiments with variable-storage quasi-Newton algorithms, *Mathematical Programming*, *45*, 407–435, 1989.

Gill, P. E., W. Murray, and M. H. Wright, *Practical Optimization*, 401 pp., Academic, London, 1981.

Harwell, Harwell subroutine library, Release 12, *Tech. Rep. Vol. 1*, AEA Technology, Oxfordshire, England, 1995.

Heras, M. de las and R. Schlitzer, On the importance of intermediate water flows for the global ocean overturning, *J. Geophys. Res.*, *in print*, 1999.

Hestenes, M. R., *Optimization Theory*, J. Wiley, New York, 1975.

Honjo, S., S. J. Manganini, and J. J. Cole, Sedimentation of biogenic matter in the deep ocean, *Deep Sea Res.*, *29*, 609–625, 1982.

Luenberger, D. G., *Linear and Nonlinear Programming*, Addison-Wesley, Reading, Mass., 1984.

Maier-Reimer, E., Geochemical cycles in an ocean general circulation model. Preindustrial tracer distributions, *Glob. Biogeochem. Cycl.*, *7*, 645–677, 1993.

Martin, J. H., G. A. Knauer, D. M. Karl, and W. W. Broenkow, VERTEX: Carbon cycling in the northeast Pacific, *Deep Sea Res.*, *34*, 267–285, 1987.

Rahmstorf, S., Bifurcations of the Atlantic thermohaline circulation in response to changes in the hydrological cycle, *Nature*, *378*, 145–149, 1995.

Redfield, A. C., B. H. Ketchum, and F. A. Richards, The influence of organisms on the composition of sea-water, in *The Sea — Vol. 2*, edited by M. N. Hill, pp. 26–77, Interscience, New York, 1963.

Riley, G. A., Oxygen, phosphate, and nitrate in the Atlantic Ocean, *Bull. Bingham Oceanogr. Coll.*, *13(1)*, 1–124, 1951.

Schlitzer, R., Determining the mean, large-scale circulation of the Atlantic with the adjoint method, *J. Phys. Oceanogr.*, *23*, 1935–1952, 1993.

Schlitzer, R., An adjoint model for the determination of the mean oceanic circulation, air-sea fluxes and mixing coefficients, *Ber. zur Polarforschung, 156*, Alfred Wegener Institute, Bremerhaven, 1995.

Schlitzer, R., Mass and heat transports in the South Atlantic derived from historical hydrographic data, in *The South Atlantic: Present and Past Circulation*, edited by G. Wefer, W. H. Berger, G. Siedler, and D. Webb, pp. 305–323, Springer, Berlin, 1996.

Schlitzer, R., Ocean Data View, http://www.awi-bremerhaven.de/GPH/ODV, 1999.

Suess, E., Particulate organic carbon flux in the oceans—surface productivity and oxygen utilization, *Nature*, *288*, 260–263, 1980.

Thacker, W. C. Three lectures on fitting numerical models to observations, *Tech. Rep. GKSS 87/E/65*, GKSS Forschungszentrum, Geesthacht, 1988.

Thacker, W. C., The role of the hessian matrix in fitting models to measurements, *J. Geophys. Res.*, *94*, 6177–6196, 1989.

Thacker, W. C. and R. B. Long, Fitting dynamics to data *J. Geophys. Res.*, *93*, 1227–1240 1988.

Volk, T. and M. I. Hoffert, Ocean carbon pumps: Analysis of relative strengths and efficiencies in ocean-driven atmospheric CO_2 changes, in *The Carbon Cycle and Atmospheric CO_2: Natural Variations Archean to Present*, edited by E. Sundquist and W. Broecker, pp. 99–110, AGU Geophysical Monograph 32, Washington D.C., 1985.

Wefer, G., E. Suess, W. Balzer, G. Liebezeit, P. J. Müller, C. A. Ungerer, and W. Zenk, Fluxes of biogenic components from sediment trap deployment in circumpolar waters of the Drake Passage, *Nature*, *299*, 145–147, 1982.

Yamanaka, Y. and E. Tajika, The role of the vertical fluxes of particulate organic matter and calcite in the oceanic carbon cycle: studies using an ocean biogeochemical general circulation model, *Glob. Biogeochem. Cycl.*, *10*, 361–382, 1996.

Reiner Schlitzer, Alfred Wegener Institute for Polar and Marine Research, Postfach 120161, 27515 Bremerhaven, Germany. (e-mail: rschlitzer@awi-bremerhaven.de)